


RESEARCH ARTICLE

Alpine greening deciphered by forest stand and structure dynamics in advancing treelines of the southwestern European Alps

Arthur Bayle¹ , Baptiste Nicoud¹, Jérôme Mansons², Loïc Francon³, Christophe Corona¹ & Philippe Choler¹

¹Univ. Grenoble Alpes, Univ. Savoie Mont Blanc, CNRS, LECA, F-38000, Grenoble, France

²Parc National du Mercantour, 23 Rue d'Italie, 06000, Nice, France

³Department of Geography, University of Bonn, Meckenheimer Allee 166, D-53115, Bonn, Germany

Keywords

dendrochronology, greening, landsat, larch, LiDAR, treeline

Correspondence

Arthur Bayle, Univ. Grenoble Alpes, Univ. Savoie Mont Blanc, CNRS, LECA, Grenoble F-38000, France. E-mail: arthur.bayle.env@gmail.com

Editor: Dr. Temuulen Sankey
Associate Editor: Dr. Wang Li

Arthur Bayle and Baptiste Nicoud are joint first author.

Received: 12 July 2024; Revised: 9 November 2024; Accepted: 16 December 2024

doi: 10.1002/rse2.430

Abstract

Multidecadal time series of satellite observations, such as those from Landsat, offer the possibility to study trends in vegetation greenness at unprecedented spatial and temporal scales. Alpine ecosystems have exhibited large increases in vegetation greenness as seen from space; nevertheless, the ecological processes underlying alpine greening have rarely been investigated. Here, we used a unique dataset of forest stand and structure characteristics derived from manually orthorectified high-resolution diachronic images (1983 and 2018), dendrochronology and LiDAR analysis to decipher the ecological processes underlying alpine greening in the southwestern French Alps, formerly identified as a hot-spot of greening at the scale of the European Alps by previous studies. We found that most of the alpine greening in this area can be attributed to forest dynamics, including forest ingrowth and treeline upward shift. Furthermore, we showed that the magnitude of the greening was highest in pixels/areas where trees were first established at the beginning of the Landsat time series in the mid-80s corresponding to a specific forest successional stage. In these pixels, we observe that trees from the first wave of establishment have grown between 1984 and 2023, while over the same period, younger trees established in forest gaps, leading to increases in both vertical and horizontal vegetation cover. This study provides an in-depth description of the causal relationship between forest dynamics and greening, providing a unique example of how ecological processes translate into radiometric signals, while also paving the way for the study of large-scale treeline dynamics using satellite remote sensing.

Introduction

Alpine ecosystems, here defined as high-elevation habitats within and above treeline, have undergone particularly fast warming in recent decades (Pepin et al., 2015, 2022), triggering diverse and extensive vegetation responses, with already tangible consequences on biodiversity and ecosystem services. This includes an increased cover of graminoids (Rogora et al., 2018) and species richness in high summits (Dentant et al., 2023; Gottfried et al., 2012; Hamid et al., 2020; Lamprecht et al., 2018; Pauli et al., 2012), shifts in phenological phases (Vitasse et al., 2021), colonization of recently deglaciated areas

(Cannone et al., 2008; Garbarino et al., 2010; Schumann et al., 2016), screes and grasslands by shrubs and trees (Cannone et al., 2007; Dullinger et al., 2004; Formica et al., 2018; Vittoz, Bodin, et al., 2008), increased shrub growth (Francon et al., 2021, 2023) and treeline upward shifts (Améztegui et al., 2010; Carlson et al., 2014; Gehrig-Fasel et al., 2007). Most studies on the dynamics of alpine plants relied on resurvey methods in real-time (Pauli et al., 2012; Rogora et al., 2018) or a space-for-time approach (Zimmer et al., 2018). For woody vegetation, dynamics are generally assessed by diachronic aerial photography comparison (Améztegui et al., 2010; Carlson et al., 2014; Gehrig-Fasel et al., 2007), dendrometry

(Dullinger et al., 2003) or dendrochronology (Cannone et al., 2022). Alpine vegetation dynamics have only more recently been studied using remote sensing techniques (Carlson et al., 2017; Choler et al., 2021, 2024; Dentant et al., 2023; Rumpf et al., 2022).

In the vast toolkit of plant ecology research, satellite remote sensing stands out due to its temporal resolution (up to daily), historical depth (spanning up to 40 years) and comprehensive spatial coverage (up to global). For decades, trends in spectral proxies of vegetation cover—most of the time referred to as ‘greening’ (positive) or ‘browning’ (negative trends)—have been used to document biotic response to environmental changes across multiple scales and have facilitated a holistic understanding of ecosystems when combined with other classical methods (Chave, 2013; Estes et al., 2018; Pettoirelli et al., 2014). However, measured reflectances and derived indices and trends are subject to biases (Bayle et al., 2024; Morton et al., 2014; Roy et al., 2016). Inconsistencies arise from various sources (such as radiometric or geometric irregularities over time) that must be accounted for to isolate the vegetation signal. In addition, translating radiometric signals into ecological information remains a complex task (Myers-Smith et al., 2020). Although vegetation indices simplify the complexity of plant life into a single dimension, and while recently developed vegetation indices (such as NIRv or kernel Normalised Difference Vegetation Index, kNDVI) offer closer ties to biophysical parameters (Camps-Valls et al., 2021), they still lack in explaining ecological processes. Attributing greening to ecological processes therefore remains a major challenge as it opens avenues to decipher the drivers and subsequent consequences of greening on other ecosystem components. This path, from the correction of the measurement and resulting metrics to the ecological interpretation, requires careful application of corrective methods to build confidence in greening estimates and the use of additional high-resolution datasets to compare the distribution of greening with underlying ecological processes.

In the French Alps, the pioneering study from Carlson et al. (2017) used long-term changes in annual maximum NDVI derived from Landsat and MODIS imagery to identify the most significant increases in annual maximum NDVI in mountains. In this lineage, Choler et al. (2021) demonstrated that north-exposed vegetation was more prone to greening compared to south-exposed slopes in the European Alps, a finding later confirmed by Rumpf et al. (2022). Yin et al. (2023) confirm these results on a global scale, showing that colder and wetter polar-facing slopes responded more positively to warming than equatorial-facing slopes. While the above-mentioned studies progressively refine our understanding of the greening of alpine ecosystems, none of them addressed the

underlying ecological process. To bridge this knowledge gap, this paper aims to decipher the spatial distribution of greening trends and underlying ecological processes in a large watershed of the Southwestern European Alps previously identified as a greening hotspot (Choler et al., 2021). For that purpose, we (1) produced a robust estimate of Landsat-based greening from 1984 to 2023 based on the state-of-the-art corrective and statistical methods, from which we (2) analysed the spatial variability of greening along gradients of elevation and slope (mesotopographic gradients). Then, by compiling a unique dataset of forest stands (tree count changes and age estimates) and structure (tree maximum height and forest vertical complexity) characteristics obtained from combined diachronic high-resolution (20 cm) aerial images, high-definition LiDAR point cloud and tree-ring analysis, we (3) investigate forest dynamics, that is forest ingrowth and treeline upward shift, and its spatial relation with greening.

Data and Methods

Study area and methods

The study area encompasses the watershed of the Col de la Cayolle (Mercantour National Park, southern French Alps, Fig. 1). According to the Strahler classification, this watershed includes five first-order catchment areas, with a total geodetic area of 64 km². Elevation ranges from 1720 m up to 3051 m a.s.l. at the Mont Pelat. However, we limited our analyses to surfaces above 2000 m to focus on vegetation within and above the treeline. Above this elevation, forest stands are dominated by *Larix decidua*. Within this study area, we gathered four independent datasets from which we derive five metrics including: the (i) Landsat time series of annual maximum kNDVI from 1984 to 2023 (*greening*), (ii) the spatial distribution of tree individuals in 1983 and 2018 (with the absolute difference referred to as *tree count changes*) obtained the photo-interpretation of a high-resolution image, (iii) *tree age estimates* derived from dendrochronological analyses from trees sampled across three of the five watersheds along an elevational gradient and (iv) forest structure metrics (*local maximum height* and *local tree height variability*) obtained using high-definition LiDAR point cloud. The procedure developed to produce these metrics of interest is schematized in Figure 2 and described in detail in the next sections.

Landsat-based greening and significance estimates

We utilized all Tier 1 data available from our study site from 1984 to 2023 in Landsat Collection 2 provided by

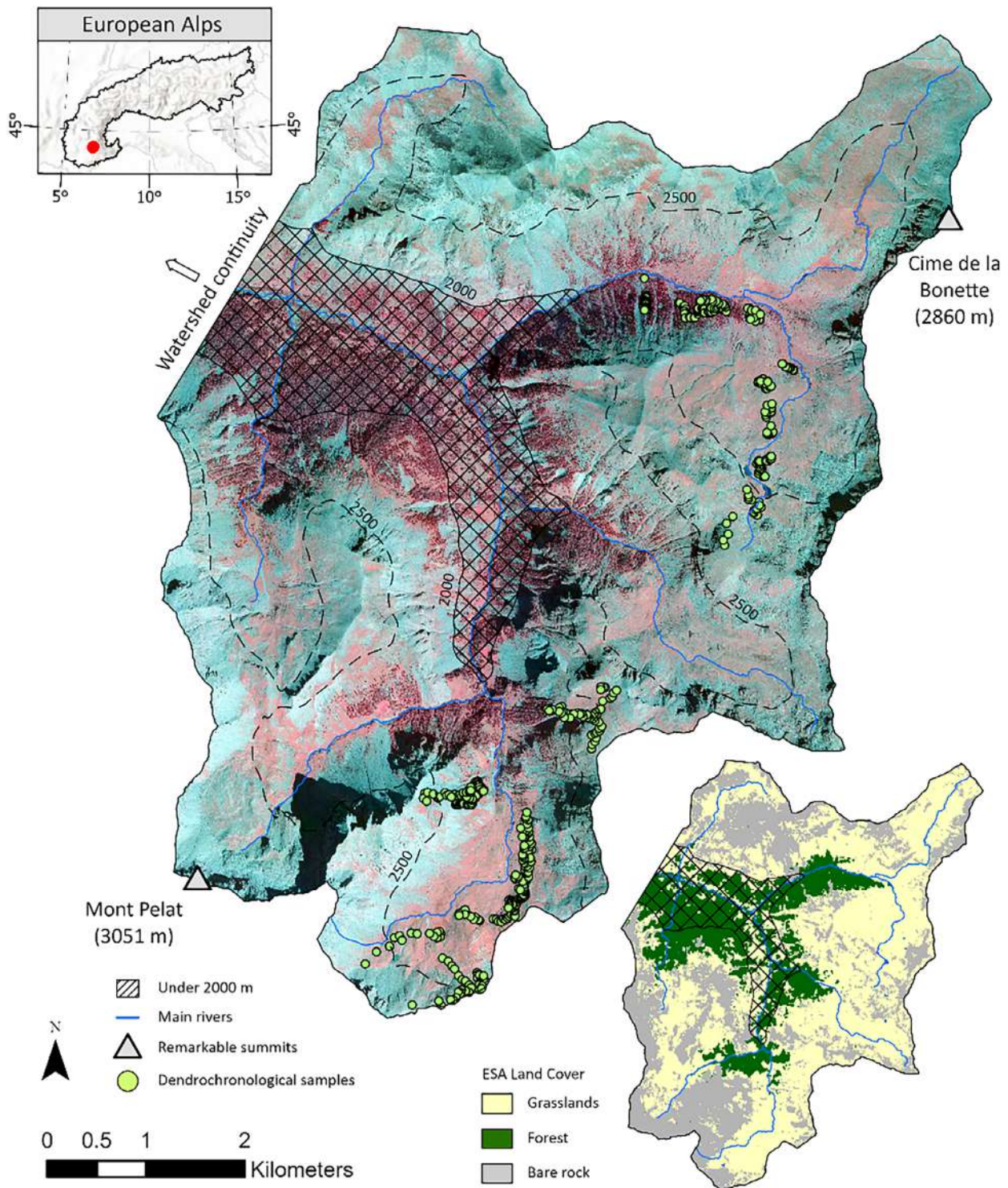


Figure 1. Very high-resolution (20 cm) infra-red coloured image of the study site, Col de la Cayolle, located in the southwestern part of the European Alps (Parc National du Mercantour). Blue lines depict main rivers originating from the 6 first-order watersheds, with the two main remarkable summits of the zone highlighted in grey triangles. The lower right inset map depicts the ESA Land cover classification for forest, grassland and bare rock. Green points on the main map show the location of the dendrochronological samples ($n = 532$).

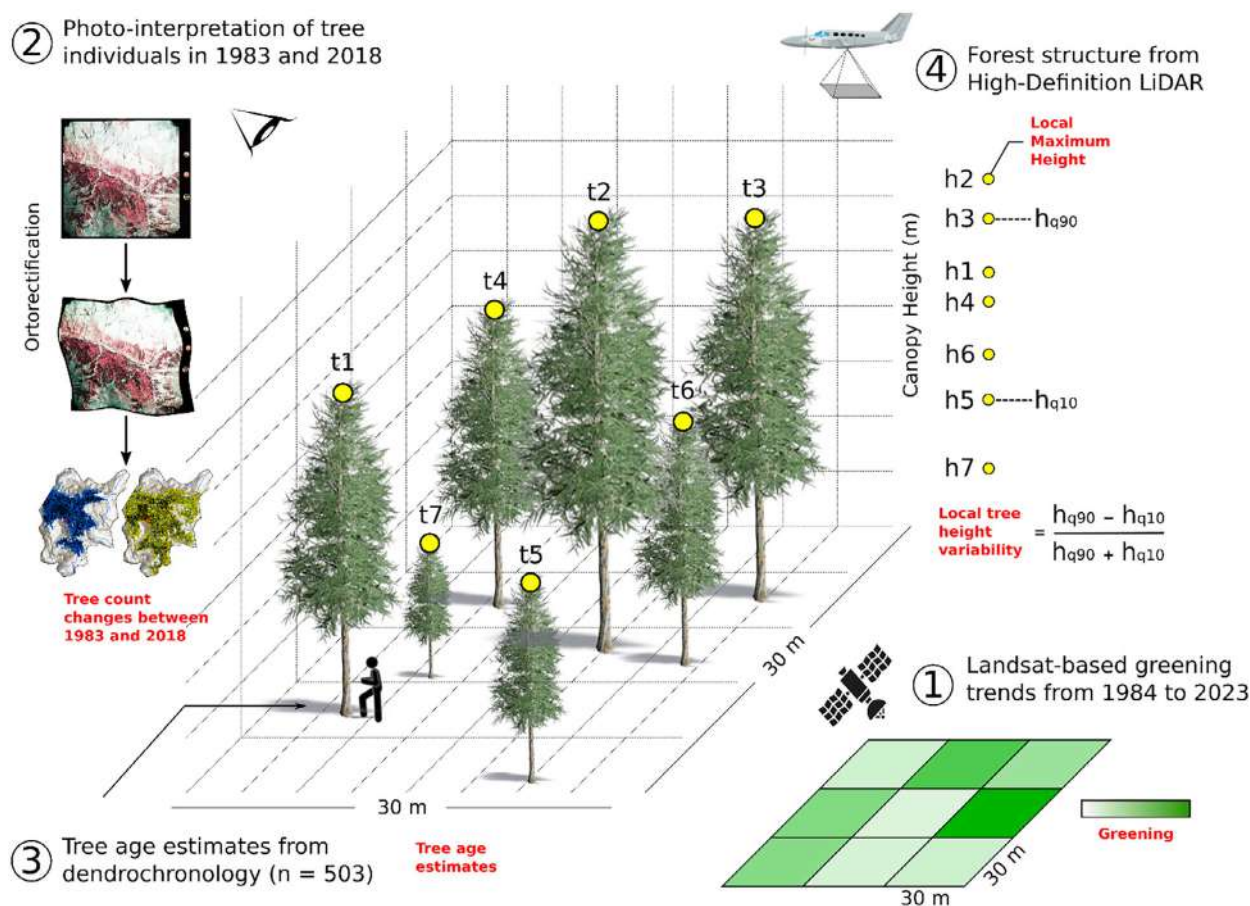


Figure 2. Schematic description of material and methods employed in this analysis following the four sections used in the text. Red text represents the five main variables extracted from our study site using different methods.

the U.S. Geological Survey (USGS) and hosted on Google Earth Engine (GEE). The Tier 1 data products analysed include surface reflectance from Landsat 5 Thematic Mapper (TM), Landsat 7 Enhanced Thematic Mapper + (ETM+) and Landsat 8 Operational Land Imager (OLI). We exclusively chose images with an average cloud cover of less than 80%, as scenes with high cloud cover can compromise the accuracy of geometric calibration, particularly for the months of June, July and August. The C Version of Function of Mask (CFmask) was applied to categorize each pixel as clear (land/water), snow, cloud, adjacent to cloud or cloud shadow (Zhu et al., 2015; Zhu & Woodcock, 2012). Pixels affected by snow, cloud, adjacent to cloud or cloud shadow were excluded from the analysis. Angular effects arising from variation in viewing and solar geometry throughout the Landsat time series have been identified as a significant source of variation in retrieved directional reflectance, independent from ground-related changes (Nagol et al., 2015). Correcting for these effects is crucial due to the variability in the

sun-surface sensor geometry, described as the Bidirectional Reflectance Distribution Function (BRDF), at the time of acquisition, which varies both spatially and temporally. Roy et al. (2016) introduced a comprehensive method using a fixed set of parameters based on the RossThick-LiSparse BRDF model (Schaaf et al., 2002). This method enables the normalization of the entire LTS to nadir (0° viewing zenith angle) and a constant solar zenith angle, reducing BRDF-related variations in reflectance. Our correction implementation involved the use of global coefficients and an optimal, normalized solar zenith angle set constant per location (Zhang et al., 2016). We performed cross-sensor calibration to correct for systematic radiometric discrepancies in red and near-infrared bands among Landsat 5 TM, 7 ETM+ and 8 OLI satellites using Berner et al. (2023) methods and coefficients from Choler et al. (2024) that were obtained for European temperate mountains. We computed the kNDVI for every cloud and snow free images available (Camps-Valls et al., 2021) using the formula:

$$\text{kNDVI} = \tan h \left(\left(\frac{\text{NIR} - \text{Red}}{2\sigma} \right)^2 \right)$$

where σ represents the pixel-wise sensitivity of the index to sparsely/densely vegetated regions computed as $\sigma = 0.5 \times (\text{NIR} + \text{Red})$ and \tanh the hyperbolic tangent function. We tracked kNDVI trajectories between 1984 and 2023 by computing the annual maximum during the growing season. Berner et al. (2020) demonstrated that NDVI-max estimates are dependent on the number of observations during the growing season. Bayle et al. (2024) showed that, because Landsat observations increase over the time series, the dependence of NDVI-max on sampling frequency can lead to an overestimation of greening. Berner et al. (2020) showed that this sampling bias can be partially corrected by modelling phenology on a pixel-by-pixel basis and adjusting the estimates of NDVI-max based on mean phenology. Hence, we applied phenological modelling to adjust kNDVI values before computing kNDVI-max. We relied on the Harmonic Analysis of Time Series (HANTS) reconstruction method as used by Choler et al. (2024). This procedure was only applied on kNDVI observations with values higher than 0.15 to eliminate unvegetated pixels as the correction relies on phenological modelling. This processing allowed us to derive a robust annual kNDVI-max series for our study site. To obtain slope and P -value estimates pixel-wise, we used an autoregressive model to derive temporally uncorrelated trends from 1984 to 2023 (Ives et al., 2021). The autoregressive model available in the 'remotePARTS' R package (Ives et al., 2021) is preferred over the commonly used Theil-Sen estimator because it considers temporal autocorrelation in time series.

Forest stands characteristics from photo interpretation and dendrochronology

Data on forest stands were obtained from two sources, (i) photointerpretation of tree individuals at the beginning and end of the Landsat time series (40 years apart) and (ii) extensive sampling and age estimation based on tree-ring counting (Fig. 2).

To pinpoint the precise locations of tree individuals in the recent period, we utilized the orthorectified version of the © BD ORTHO Coloured Infra-red image from 2018, available in Lambert-93 (EPSG:2154) projection, which was already orthorectified and georeferenced. For the earlier period (i.e. 1983), we mosaicked infra-red coloured aerial images downloaded at remonterletemps.fr. These images correspond to a unique acquisition campaign in June 1983. We manually geo-referenced and oriented nine historical aerial images. Following Bayle (2020), we

orthorectified and georeferenced each image using ArcGIS Pro software (Esri, 3.2.0), specifically employing the spline transformation method with the 2018 image as a reference. The spline method is a true rubber-sheeting method that ensures that all control points in the reference map are geo-referenced to the exact coordinates provided for these locations. This method was preferred over parametric approaches, which require the interior and exterior parameters, as the nine images were distorted in various ways due to inconsistent view angles and high variations in elevation. Additionally, it gains substantial advantages from the abundance of available control points. For each of the nine images, we followed the same three-step procedure: (1) 10–50 features providing stable and easily identifiable reference points in 1983 and 2018, such as roads, topographic features or houses were used as a reference to align the orthorectified imagery accurately; (2) up to 150 control points per image were added, starting at the edges and moving progressively toward the centre of the image. This method ensures excellent accuracy and the most consistent possible error across the entire image but requires a large amount of operator time; (3) overlapping areas between adjacent images were finally used to adjust the georeferencing, in accordance with the reference image. Since Root Mean Square Errors are not computable with the spline transformation method due to the exact placement of control points, we visually validated the orthorectification and georeferencing steps by superimposing processed images. Once geo-referenced, the average spatial resolution of 1983 images was 40 cm.

Tree individuals were manually photo-interpreted from processed images on ArcGIS Pro software (Esri, 3.2.0) for the two dates. The study area was divided into 1×1 km squares with each square photo-interpreted one at a time. Points that have already been photo-interpreted were systematically displayed on the screen during photo-interpretation so that double counting was hardly possible. To minimize operator biases, photo-interpretation was primarily conducted by a single observer (A.B.), with contributions from B.N. Manual photo interpretation is a time-consuming process and can lead to variations due to training biases. To ensure consistent photo interpretation quality across our study area, the areas that were photo-interpreted initially were reviewed a second time by the primary interpreter only (A.B.). Errors related to double mouse clicking were identified during the photo-interpretation process and corrected. In addition, we calculated the exact coordinates of each point and removed duplicated values. This diachronic analysis of high-resolution aerial images allowed us to obtain a precise and exhaustive trajectory of tree individuals in our study area over the Landsat acquisition period. We summarized the distribution of tree individuals by counting the number of trees per Landsat pixel (30×30 m), which we refer to as 'tree count'.

To enhance the temporal resolution of the tree dynamic, we complemented the diachronic analysis with dendrochronological analysis. Sampling campaigns were conducted over 3 years (2021, 2022 and 2023), targeting larch trees across five elevational transects. The transects extend from the dense forest stand located ~ 2000 m a.s.l. to the highest tree individuals (~ 2700 m). They were positioned to cross patches with intense greening, to account for varying exposure, slope and grazing influences, in the different watersheds of our study site. We systematically sampled the dominant trees at regular intervals along the elevation gradient. Increment cores were extracted from 532 trees using a Pressler increment borer. To precisely estimate tree age, cores were taken as close as possible to the soil surface. All collected samples were air-dried, mounted and prepared following standard dendrochronological procedures described by Bräker (2002). They were subsequently scanned at 2400 DPI using an Epson 10000 XL Scanner. Tree-ring width series were produced measuring the rings on the high-resolution images using the program *CooRecorder*, and visual cross-dating was undertaken on *CDendro* 7.6 software (Larsson, 2013). The pith offset, that is, the number of rings from the pith to the last cross-dated ring, was estimated using the “DistanceToPith” tool in *CooRecorder*, based on the concentric circles method. While a significant pith offset may lead to an underestimation of ages in older individuals, we anticipate minimal bias given the predominantly young age and limited diameter of the majority of sampled trees.

Forest structure from dense LIDAR

Data on forest structure were obtained for the end of the Landsat time series from the high-density point clouds IGN LiDAR HD from the French lidar High-Density (LiDAR HD) campaign (<https://geoservices.ign.fr/lidarhd>) collected in summer 2021 over our study site. Across our study site, the average point density is 26.4 points/m², with 24 pulses/m² and a total of 5.55 billion points covering the entire watershed. The point cloud was processed using the ‘lidR’ R package (Roussel et al., 2020). As a first step, we normalized point height using Delaunay triangulation for spatial interpolation with default parameters. Next, we constructed a canopy height model (CHM) using a normalized point cloud through the points-to-raster method with default parameters. Finally, we extracted the apex tree height for each of the individuals identified through photointerpretation on the 2018 aerial image (Forest stands characteristics from photo interpretation and dendrochronology Section).

For each Landsat pixel (30 × 30 m), we extracted two metrics representing the forest structure in recent years:

(1) the local maximum height and (2) the local tree height variability. The latter is calculated as the normalized difference between the ninth and the first quantile of the tree height distribution within each Landsat pixel (Fig. 2). This index tends to be closer to one when there is a greater difference between the smallest and tallest tree heights within a pixel, and closer to zero when this difference is lower. It represents the homogeneity of forest structure within each pixel. We preferred using a quantile instead of a simple standard deviation as it is less sensitive to extreme values. As the data is only available for the year 2021, it is interpreted as an indicator of the forest structure at the end of the Landsat time series.

Statistical analysis

We performed three distinct analyses corresponding to (1) detection, (2) attribution and (3) ecological interpretation of the greening signal.

1. We explored the distribution of Landsat greening direction and magnitude across mesotopographic gradients defined by elevation data obtained from the 25 m EU-DEM (<https://land.copernicus.eu/imagery-in-situ/eu-dem/>) and Diurnal Anisotropic Heat Index (DAH) resampled on Landsat grid using bilinear interpolation. The DAH index approximates the anisotropic heating of the land surface due to radiation (Böhner & AntoniĆ, 2009). We computed DAH as $\cos(\text{amax} - a) \times \arctan(b)$, where a is the aspect, b is the slope and the parameter amax corresponds to the aspect with the maximum total heat surplus. We used the default amax value of 202.5° in SAGA 7.8.2. Values closer to -1 have low radiation energy (steep north-exposed slopes) while values closer to $+1$ have high radiation energy throughout the day (steep south-exposed slopes). Values around 0 represent flat surfaces.
2. We explored the attribution of greening to ecological processes by comparing greening to changes in tree count within similar mesotopographic gradients. For this purpose, we split Landsat pixels showing significant greening ($P < 0.05$) into those attributed (with changes in tree count) and those not attributed (without tree count changes, including the absence of tree in both periods) to forest dynamics.
3. We deciphered patterns of greening attributed to forest dynamics using tree count changes, tree age estimates and forest structure metrics (local maximum height and normalized variability). To achieve this goal, we (Spatial distribution and attribution of greening Section) examined the distribution of each variable along elevation. Next, we (Causal relationships between greening, forest stands and structure dynamics Section)

implemented two random forest analyses and partial dependence plots to identify the best predictors of greening. For the first analysis, we built a pixel-based random forest using only tree count changes, local maximum height and local maximum normalized variability as predictors of greening to maximize the number of samples used. The second analysis involved building a sample-based random forest where we extracted greening, tree count changes, local maximum height and local maximum normalized variability at the location of dendrochronological samples. This allowed us to include tree age estimates in our analysis. Variance explained and variables importance presented in the results section are derived from this second model. We computed each random forest 100 times by randomly selecting two-thirds of the dataset to obtain uncertainty estimates. Partial dependence plots were generated to assess how greening trends varied across the range of the predictor while holding all other predictors at their average value. We computed the quantiles of greening values, elevation and proportion for each category of pixel including non-significant pixels, significant greening, significant greening attributed to forest expansion and significant greening not attributed to forest expansion. All the analyses were performed using the randomForest, caret and pdp R packages (Greenwell, 2017; Kuhn et al., 2023; Liaw & Wiener, 2002). Finally, we present a synthetic view of the relationships between greening and advancing treelines.

Results

Spatial distribution and attribution of greening

We observed high variability in the spatial distribution of greening magnitude (Fig. 3A) with the highest magnitudes observed on north-exposed slopes between 2100 and 2300 m (0.005 kNDVI_{max}/year, Fig. 3B). In total, 61.5% of the watershed area above 2000 m. shows significant greening ($P < 0.05$), although with pronounced spatial disparities (Fig. 3C and D). On north-exposed slopes between 2100 and 2300 m, nearly 100% of the pixels exhibited significant positive greening (Fig. 3D), whereas this percentage decreases to 60% between 2300 and 2700 m. By contrast, on south-exposed slopes, the proportion of pixels showing significant greening is higher above (60%) than below (45%) 2400 m (Fig. 3D). The number of tree individuals more than doubled over the Landsat acquisition period with 140 210 trees identified in 1983 compared to 355 011 in 2018 (Fig. 4A). Increases in tree individual count were observed for all elevation and

exposition in the watershed, but with a maximum between 2100 and 2300 m, mainly on north-exposed slopes (Fig. 4B). Based on the presence/absence of tree count changes, we attributed significant greening to either 'forest dynamics' or 'other ecological processes'. Across the entire watershed, we found that 56% of significant greening coincided with an increasing number of identified trees, while greening was attributed to other ecological processes for 44% of the pixels. (Fig. 5A). Along mesotopographic gradients, the proportion of greening attributed to forest dynamics reaches 90% in north-exposed slopes of the subalpine belt (between 2000 and 2300 m above sea level) compared to 70% in south-exposed slopes at similar elevations (Fig. 5B). Between 2400 and 2500 m, this proportion decreases to 30%, and it is nearly absent above 2500 m (Fig. 5B).

Causal relationships between greening, forest stands and structure dynamics

The distribution of tree count changes shows a maximum between 2150 and 2250 m coinciding with local maximum tree recruitment mostly occurring between 1980 and 1990 (Fig. 6A). The oldest tree individuals measured were established around the year 1985 at an elevation of 2150 m. Progressively between 2150 and 2300 m, the establishment year changes from 1985 to 2000. Above 2300 m, all trees sampled were found to have been established around the year 2005 (Fig. 6A). The local maximum tree height progressively decreases from 16 m at 2000 m to 2 m at 2600 m. At around 2200 m, the highest tree height is approximately 10 m (Fig. 6B). The local tree height normalized variability slightly peaks around 2000 m with the lowest variability observed above 2350 m and moderate variability under 2100 m (Fig. 6B). As previously shown in Figure 3, greening is peaking around 2200 m (Fig. 6C).

The random forest model including the four predictor variables explains 74.30% of the variance in greening. Tree count changes were the most important variable in explaining these trends, followed by local tree maximum height, local tree height variability and establishment year, in decreasing order of importance. We used partial dependence plots to explore the relationship between each variable and greening while removing the effect of other predictors. Greening shows progressive increase, ranging from 0.0031 NDVI/year when there are no changes in tree count to 0.0045 NDVI/year in areas with the highest tree count change between 1983 and 2018 (Fig. 7A). Trees recruited between 1980 and 1990 exhibit consistently high greening at 0.00425 NDVI/year, whereas younger trees recruited after 2005 show lower trends at 0.00375 NDVI/

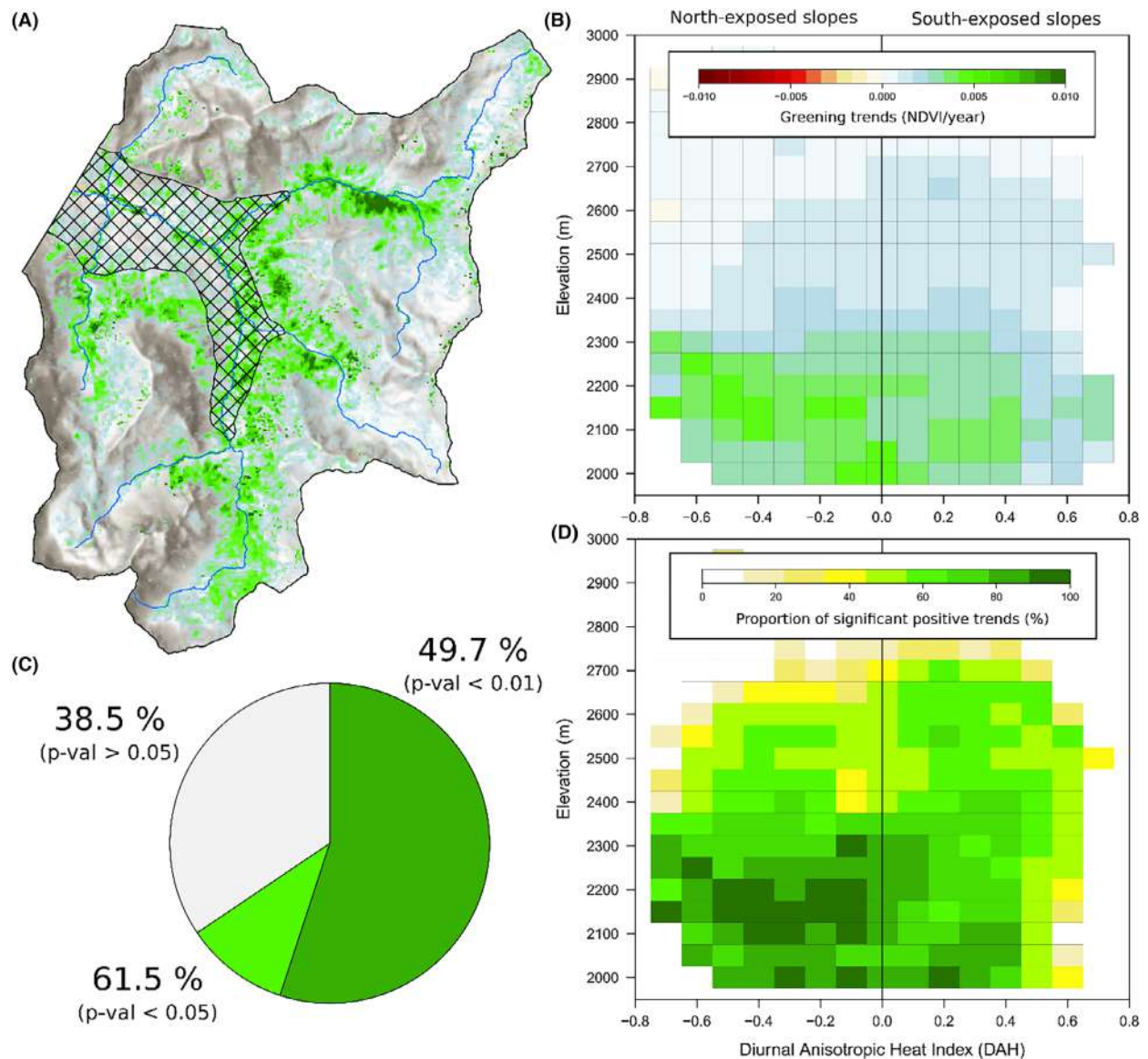


Figure 3. (A) Distribution of Landsat-based greening trends over our study site. (B) Distribution of average greening trends along gradients of elevation and aspect for all pixels in the study site. Cells in white have less than 10 pixels and are not shown. (C) Percentage of significant positive trends over the whole area. (D) Distribution of the percentage of significant positive trends along elevation and aspect gradients for all pixels in the study site.

year but with greater variability (Fig. 7B). Greening is highest for stands dominated by tree of moderate height around 15 m (0.0045 NDVI/year), moderate for taller trees around 30 m (0.0037 NDVI/year) and lower for smaller trees around 5 m (0.003 NDVI/year) (Fig. 7C). Greening peaks when local tree height variability is highest, 0.00385 NDVI/year compared to 0.00325 NDVI/year for low local tree height variability (Fig. 7D). To summarize, our findings indicate that greening is tightly associated with forest stands dominated by 30–40 years-old trees, exhibiting high variability in tree height (around a

median of 15 m) and having undergone a strong increase of the number of trees in the last four decades (Fig. 8). We found that pixels exhibiting significant greening not attributed to forest expansion had greening values of 0.0017 NDVI/year [0.0011/0.0025] compared to 0.0031 NDVI/year [0.0021/0.0045] for those attributed to forest expansion. Within greening pixels attributed to forest expansion, we found high variability among pixels with the highest values reaching 0.0056 NDVI/year [0.0038/0.0076] for pixels corresponding to forest stands dominated by 30–40 years-old trees, high variability in tree

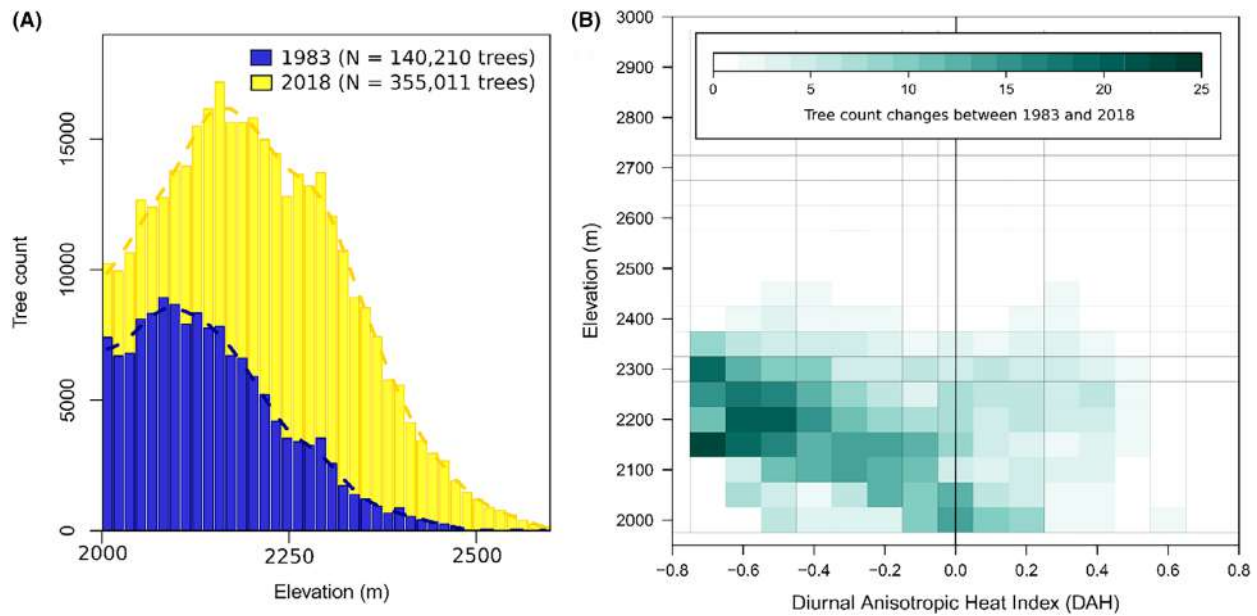


Figure 4. (A) Number of photo-interpreted trees along elevation for 1983 and 2018. (B) Distribution of absolute tree count changes between 1983 and 2018 along gradients of elevation and DAH.

height and high increase in tree count number (Table 1). In older and younger stands, greening values were around 0.003 NDVI/year [0.0025/0.0046].

Discussion

Studies on plant dynamics using satellite imagery often face challenges in interpreting results ecologically. This paper addresses these challenges by developing a statistically robust method to estimate greening (Fig. 3) and comparing it with datasets describing trajectories of forest stands and structure (Fig. 2). Previous studies have identified the south-western European Alps, especially the sparsely vegetated north-facing subalpine areas around 2200 m, as greening hotspots (Choler et al., 2021; Rumpf et al., 2022). We found similar patterns over the Cayolle watershed (Fig. 3), indicating that our study site is representative of this hotspot. We found that the spatial variability of greening is mostly driven by forest dynamics (Fig. 4), with more than half of the greening attributed to changes in tree count over the watershed, and almost all of it for subalpine north-exposed (Fig. 5). This indicates that the dynamics of the advancing treeline are the primary cause of the observed intensified greening in this area. By mobilizing a unique assemblage of datasets on tree count changes, age and forest structure (Figs. 2 and 6), we identified the specific moment, within the forest successional stage, that coincides with the highest greening magnitudes (Fig. 7). This corresponds to an intermediate stage of advancing treelines, with stands composed

of 40 years old, tall trees and ongoing closure of clearings by younger individuals (Fig. 8). The contributions of this paper are threefold: (1) forest dynamics are the predominant factor contributing to greening in the south-western Alps; (2) for a given stage of forest succession, the greening peaks occurs when the vertical growth of the early established trees coincides with the closure of clearings by younger individuals leading to a notable expansion of both vertical and horizontal vegetation cover; (3) greening is a reliable indicator for monitoring forest dynamics across extensive geographical scales and over prolonged periods, potentially spanning decades.

Attributing alpine greening to ecological processes

This detailed analysis of how satellites capture ecological processes is conceptually part of the approach to move beyond the diagnostic of change (production of greening maps and identification of hotspots and spatial patterns) toward the attribution to underlying ecological processes. In a given area, several ecological processes can take place simultaneously, all potentially resulting in an increase in NDVI of comparable magnitude. However, the drivers of these processes and the consequences can vary greatly. We demonstrate that within the study area, forest dynamics account for the majority of the greening, although in certain locations, particularly at higher elevations, more than half, or even all, of the greening is attributed to other ecological processes (Fig. 5B).

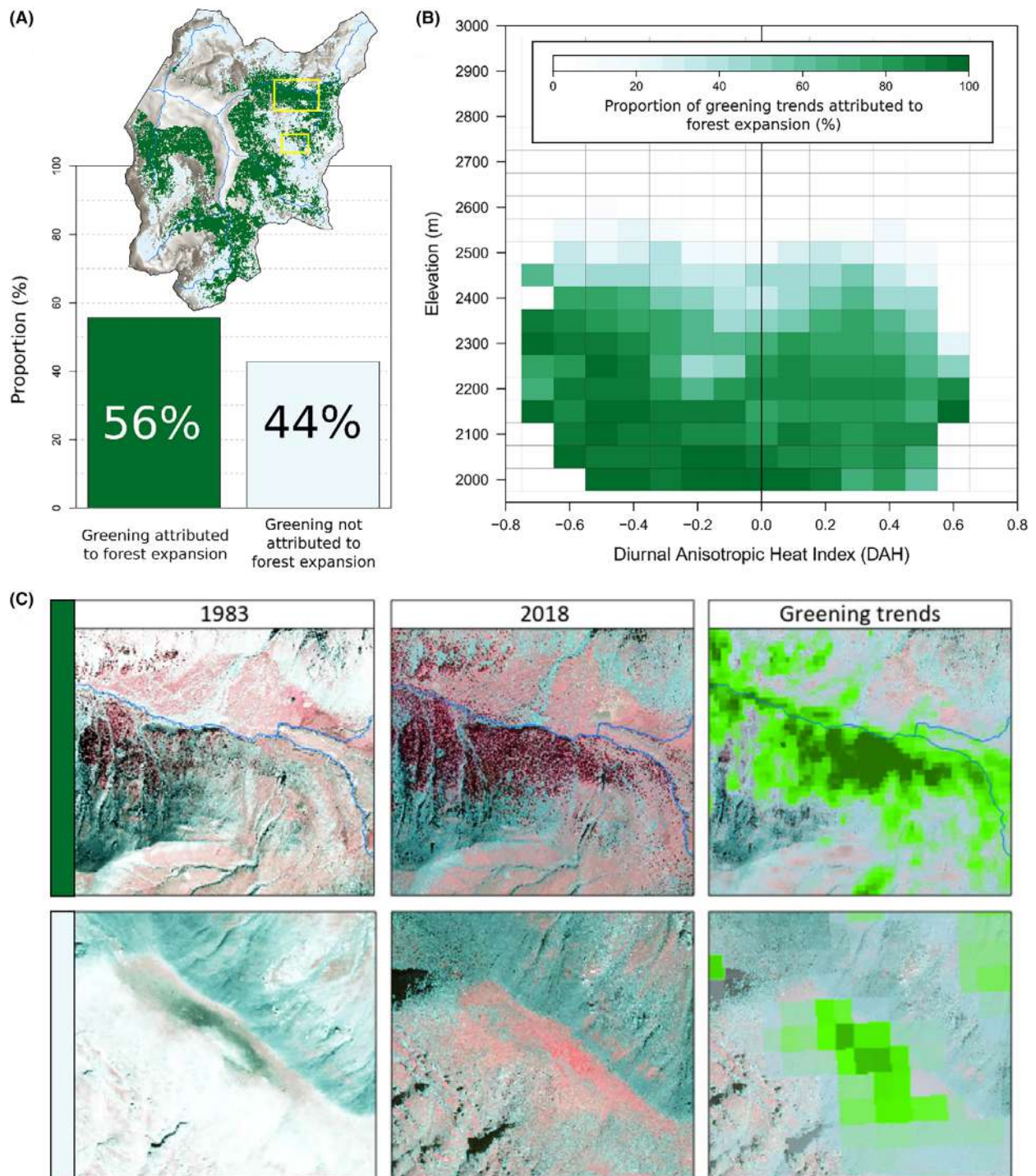


Figure 5. (A) Distribution and proportion of pixels with significant greening trends ($P < 0.1$) associated with tree count change with inset map for (C). (B) Proportion of greening trends attributed to tree count changes along mesotopographic gradients. (C) Examples of very high-resolution infra-red colours images from 1983 (40 cm) and 2018 (20 cm) and greening trends over two sites highlight the overlapping trajectories of treeline and greening trends.

For example, we have identified a summit grassland around 2600 m which was degraded in 1983 but has since recovered by 2018 (Fig. 5C). This grassland, historically used

as a sheep resting place before the return of wolves in the late 1990s, shows high greening rates, reaching up to 0.008 NDVI/year, surpassing the average greening observed in

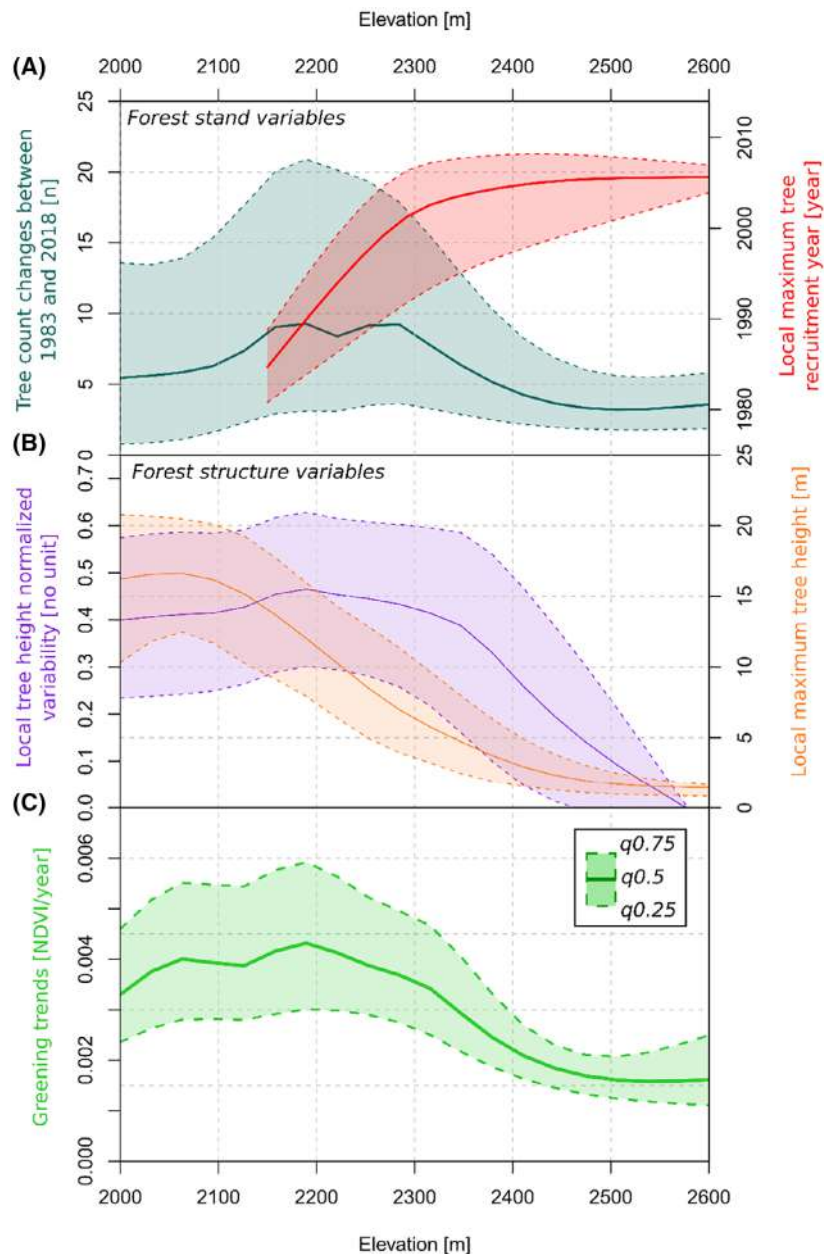


Figure 6. Distribution of (A) forest stands (tree count changes and tree recruitment year), (B) forest structure (local tree height variability and maximum) variables and (C) greening variable along elevation gradients for pixels exhibiting significant greening attributed to tree trajectories. Solid and dashed lines represent the median, and quantile 25 and 75 values respectively obtained from quantile Generalized Additive Models (qGAM).

advancing treelines at lower elevations. Similarly, in a wider alpine context, several studies confirm that distinct ecological processes could be reflected in a closely related radiometric signal. Dentant et al. (2023) thus linked intense greening (up to 0.004 NDVI/year) to increases in plant species richness attributed to the upward migration of competitive species on high-elevation nunataks of Mont-Blanc. In proglacial margins, Bayle et al. (2023) attributed the high magnitude of

greening (up to a maximum of 0.01 NDVI/year) to the opening of new surfaces for colonization and slope stabilization following deglaciation (Eichel et al., 2023). Large-scale studies such as those of Choler et al. (2021) or Rumpf et al. (2022) in the European Alps encompass numerous ecological processes. However, there is no doubt that the variables driving these ecological processes differ from one another. Failure to consider these processes independently

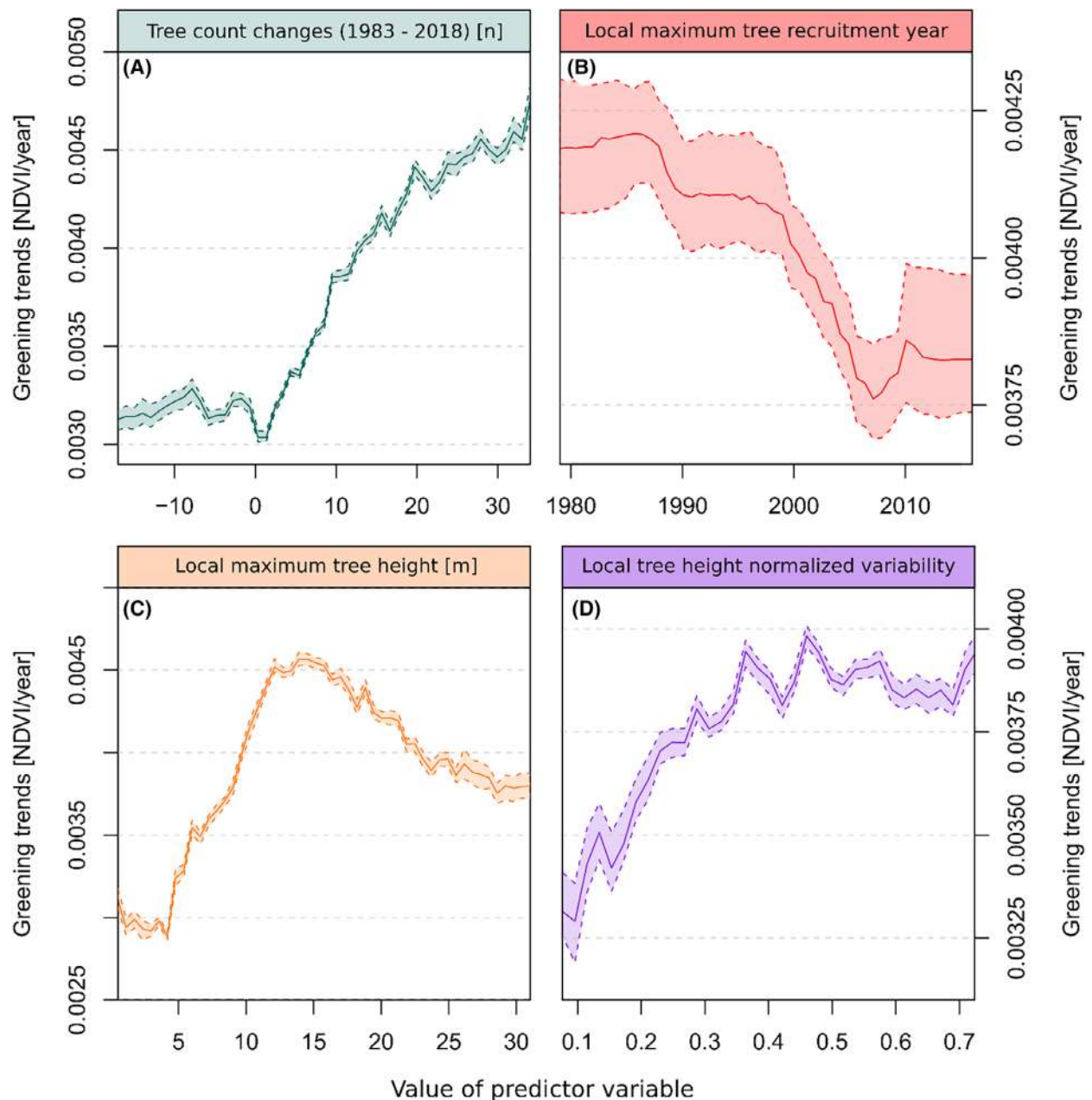


Figure 7. Partial dependence plots of predictor variables in a Random Forest regression model. Solid and dashed lines represent the median, and quantile 25 and 75 values respectively obtained by recomputing the analysis using randomly 66% of the dataset each time.

necessarily results in oversimplification and may lead to misinterpretation of both causes and consequences of the greening complexity (Myers-Smith et al., 2020).

Temporality of satellite observations in advancing treelines

Forest development typically follows successional stages that have been widely discussed and theorized (Oliver &

Larson, 1996), leading to variations in tree count, age, height or structure complexity over space and time (van Ewijk et al., 2011). Along the elevational gradient, we identified several stages including mature stands comprising multi(centennial)-old tall trees with moderate structural complexity and limited changes in tree count at lower elevations (Fig. 6). On the other hand, high elevations stands are in a pioneering stage, characterized by young and small trees, sparsely distributed and with limited height variations.

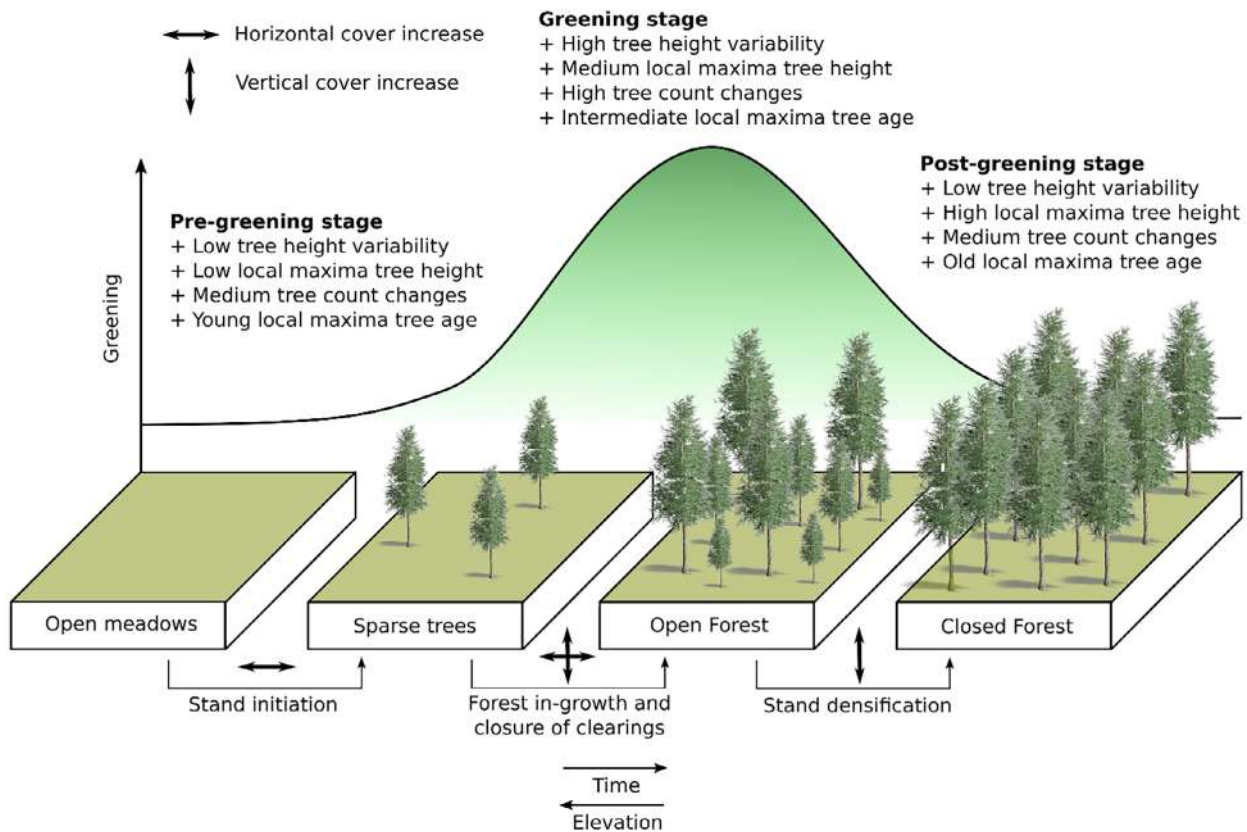


Figure 8. Link between forest successional stage and forest stands and structure characteristics and its translation into greening. Four forest successional stages are distinguished with the main processes of forest in growth and expansion underlined. Greening magnitude is interpreted in light of the transition between forest successional stages (and corresponding changes in vegetation cover), suggesting the existence of pre-greening, greening and post-greening stages in the context of advancing treelines.

In the central portion of the gradient, larch forest typically represents an intermediate stage with 40-year-old tall trees and the ongoing closure of clearings by younger individuals, resulting in high complexity in forest structures (Fig. 6). Among those stages, greening is found to be the highest in areas currently exhibiting the intermediate stage (Fig. 7). This suggests that Landsat-based accounts of greening peaked when the initial establishment occurred ~ 40 years ago, at the beginning of the Landsat time series. Consequently, other greening estimates based on sensors such as MODIS would fail to capture this peak. During this period, trees from the initial wave of establishment have increased in height and the density of the understory strata has risen (Fig. 8), corresponding to both increased horizontal and vertical vegetation cover (Myers-Smith et al., 2011). In this context, we can reasonably hypothesize that older stands below 2100 m a.s.l. represent a post-greening stage, which would have been identified as a greening hotspot in an earlier time window. Conversely, we expect higher-elevation grasslands undergoing initial establishment to show increased greening magnitude in the coming decades,

assuming favourable environmental conditions persist (Fig. 8). Landsat-based greening is measured between 1984 and 2023, representing a snapshot within the true but unknown temporal scale at which ecological processes unfold. Consequently, the sensitivity of remote sensing measurements significantly relies on the kinetics of the underlying processes, and whether they generate a sufficiently significant signal during this limited 40-year observation period. In the European Alps, landscapes have been shaped by human activity for thousands of years (Giguët-Covex et al., 2014; Pini et al., 2017). In the southern French Alps, the earliest stone structures associated with pastoralism, dating to ca. 2500 BC, are found at elevations between 2100 and 2400 m (Walsh, 2015) presupposing forest clearance designed to create more suitable pasture. These practices have continued throughout the Holocene with varying intensity (Giguët-Covex et al., 2014). After a period of expansion following the Black Death, the French forest contracted almost continuously, reaching a minimum in the early 19th century, followed by an increase in forest cover up to the present (Mather et al., 1999; Meyfroidt

Table 1. Summary of greening values and proportion of greening pixels. Non-significant and significant pixels correspond to pixels with a $P > 0.01$ and $P < 0.01$, respectively, with the proportion being relative to the entire study area. Significant greening attributed, or not, to forest, expansion corresponds to pixels exhibiting significant greening ($P < 0.01$) and with changes, or no changes, in tree count between the two periods. Within greening pixels attributed to forest expansion, we distinguished the three stages (pre-greening, greening and post-greening) described in Figure 8. Values correspond to the median and first and third quantiles.

Pixel categories	Greening values (NDVI/year)	Proportion (%)	Elevation (m)
Non-significant ($P > 0.01$)	0.0005 [0.0001/ 0.0012]	51	2499 [2376/ 2621]
Significant greening ($P < 0.01$)	0.0024 [0.0015/ 0.0036]	49	2364 [2224/ 2517]
Significant greening attributed to forest expansion	0.0031 [0.0021/ 0.0045]	56	2268 [2152/ 2369]
Pre-greening stage	0.0035 [0.0025/ 0.0047]	37	2306 [2239/ 2360]
Greening stage	0.0056 [0.0038/ 0.0076]	37	2193 [2133/ 2257]
Post-greening stage	0.0032 [0.0024/ 0.0044]	26	2085 [2044/ 2134]
Significant greening not attributed to forest expansion	0.0017 [0.0011/ 0.0025]	44	2525 [2395/ 2613]

et al., 2010; Meyfroidt & Lambin, 2011). Landsat-based greening and associated forest expansion over the last four decades hence only capture the most recent moment of this multi-centennial trajectory.

Greening as a proxy for shifting treelines

One of the most striking ongoing ecological trajectories in alpine ecosystems worldwide is the upward shift of treelines (Devi et al., 2008; Harsch et al., 2009; Liang et al., 2011). This phenomenon is an extensively observed ecological trend in the European Alps (Anselmetto et al., 2024), with well-documented case studies in the central Austrian and Italian Alps (Malfasi & Cannone, 2020; Tasser et al., 2007), Switzerland (Gehrig-Fasel et al., 2007; Vittoz, Rulence, et al., 2008) and France (Didier, 2001). Similar trends are reported in neighbouring mountain ranges including the Pyrenees (Camarero et al., 2018; Camarero & Gutiérrez, 2004), the Apennines

(Garbarino et al., 2023; Vitali et al., 2018) and the Carpathians (Kucsicsa & Bălăceanu, 2020). Despite extensive studies, the spatial variability in the magnitude of treeline changes remains puzzling with contrasting kinetics of treeline trajectories observed in the European Alps (Dinca et al., 2017). In particular, the interactions between the factors driving treeline shifts, such as climate, topography, species distribution and geomorphological activity, remain unclear. Most studies exploring treeline shift have relied on repeated field surveys, diachronic series of maps or photographs or dendrochronology, thus limiting the surface area from which conclusions can be drawn. Using greening as a proxy for advancing treelines offers a simplified and scalable approach (Garbarino et al., 2023; Wei et al., 2020). This perspective partly aligns with the results of Bolton et al. (2018) who explored the distribution of Landsat-based greening along forest structure gradients and observed faster changes at the ecotone compared to closed forest and open lands. Similarly, Berner and Goetz (2022) tracked greening along gradients of tree cover density at the Boreal biome scale and found a signal consistent with a poleward biome shift. Yet, both studies relied on spatial co-occurrence rather than causal evidence, leading to results that have sparked controversy due to discrepancies with field studies (Timoney, 2022). This calls for an improved understanding of how advancing treelines translate into greening signals.

Here, we address this knowledge gap by providing a better understanding of how the population and structural trajectory of an advancing treeline influence the magnitude of greening. Our results not only confirm the validity of greening as a proxy for advancing treelines but also enable exploration of their large-scale drivers. Additionally, while we are considering greening as a single monotonic trend over the last four decades, tracking interannual variability of maximum NDVI might highlight non-linear trajectories of forest expansion (Bayle et al., 2022). This is significant as forest expansion might have occurred at an irregular rate during this period considering that warming mostly occurred in the 1990s. Furthermore, the reappearance of wolves in the 1990s (Campion-Vincent, 2005) led to changes in sheep practices, which potentially influenced the treeline movement (Espuno et al., 2004). Beyond greening, studying the temporal variability of NDVI_{max} trends could improve our understanding of the intertwined effects of climate and land-use change over the last four decades.

Limits of datasets and analysis

In this study, we mobilized four independent datasets to characterize stand and forest structure, each with its limitations and inaccuracies. Diachronic analysis of aerial

photographs has been used to study treeline movement by either image classification approach (Carlson et al., 2014; Vitali et al., 2018) or manual and machine-based photo interpretation of tree individuals (Treml et al., 2016). Our photointerpretation was conducted manually on two sets of images with differing spatial resolution, radiometric quality and taken, at different times of day. We found that our ability to identify smaller trees and differentiate them from larger bushes depended significantly on the shade cast by the tree. During field sampling, we realized that trees smaller than 1 m 50 were not identifiable on the 2018 images, with this threshold likely being slightly higher on older images, leading to overestimation of tree count changes between both periods. This bias could limit our interpretation of the association between greening and forest succession (Fig. 8), as we cannot confirm that trees newly present in 2018 were not simply small and undetectable in 1983.

Nevertheless, our analysis also relied on tree dating by coring at the base to determine the date of recruitment (Fig. 2). This approach allows us to quantify the age gradient along greening and altitude with confidence (Fig. 6), although the absolute age of the trees is probably slightly underestimated due to pith missing during the coring process (Wong & Lertzman, 2001) and our sampling only covers a limited part of our study site (Fig. 1). Similarly, the forest structure metrics we relied on are simplified proxies. Based on our LiDAR dataset, with an average point of 26.4 points/m², we could not compute more accurate metrics such as the Vertical Complexity Index (van Ewijk et al., 2011) as in Gril et al. (2023). Additionally, forest structure metrics were computed at the Landsat-pixel scale (30 m) to match other data, but this scale might not be ideal for capturing forest structural diversity (Atkins et al., 2023).

Despite these limitations, we are confident that our study provides a detailed interpretation of greening in ecological terms. However, transposing these findings to other mountain regions remains challenging. The advancement of the treeline at our study site is particularly rapid and consists entirely of Larch trees, known for their pioneering capacity due to rapid growth, short time between germination and sexual maturity and anemochorous seeds (Fourchy, 1953). The sensitivity of the remote sensing measurements significantly relies on the kinetics of the underlying process, and whether it generates a sufficiently significant signal during the 40-year observation period. For example, we cannot assert that the widely studied *Pinus uncinata* advancing treeline will produce a similar signal, given its much longer reproduction times and spread by zoochory. Additionally, considering the current elevation of the *P. uncinata* treeline at

around 2000 m, climatic control on forest expansion is expected to be limited (Gehrig-Fasel et al., 2007). Further studies in different contexts, including other treeline-forming tree species, varying rates of expansion and at different elevations or latitudes, particularly closer to the climatic treeline, are needed to better understand the complex link between the radiometric signal and advancing treelines.

Conclusion

In this study, we quantified Landsat-based greening over the last four decades in a large watershed of the South-western Alps, an area identified as a hotspot of greening at the scale of the European Alps. Using a heterogeneous and multidisciplinary dataset compiled for a single area, we demonstrated that more than half of significant greening in the watershed is attributed to forest dynamics, though there is considerable variation in greening magnitude within advancing treelines. Greening is found to be particularly high when the initial establishment occurred at the beginning of the Landsat time series; During the observation period, this first wave of recruitment has grown while the understory strata have been re-colonized by other trees, leading to increased horizontal and vertical vegetation cover. These new findings provide valuable insights into the ecological processes underlying alpine greening and offer an opportunity to study treeline dynamics at a large scale using greening as a proxy.

Acknowledgements

The authors are particularly grateful to the Parc National du Mercantour for their support, authorization and helpful discussion during fieldwork. A.B. acknowledges a CNRS doctoral scholarship. This work received funding from the ANR project TOP (LIFE16 CCA/IT/000060) and the Zone Atelier Alpes project HERITAGE. This research has been supported by the Agence Nationale de la Recherche (project TOP, Trajectories of agrO-Pastoral systems in mountains, grant no. ANR-20-CE32-0002). LECA acknowledges the Agence Nationale de la Recherche (grant nos. Labex OSUG@2020 and IA-10-LABX-0056).

Author Contributions

A.B. designed the methodology, conducted the remote sensing analysis and wrote the original draft. B.N. conducted the dendrology and contributed to photointerpretation. C.N., L.F. and P.C. participated in the analysis and manuscript editing. J.M. organized and participated in the fieldwork.

References

- Améztegui, A., Brotons, L. & Coll, L. (2010) Land-use changes as major drivers of mountain pine (*Pinus uncinata* Ram.) expansion in the Pyrenees. *Global Ecology and Biogeography*, **19**(5), 632–641. Available from: <https://doi.org/10.1111/j.1466-8238.2010.00550.x>
- Anselmetto, N., Weisberg, P.J. & Garbarino, M. (2024) Global change in the European Alps: a century of post-abandonment natural reforestation at the landscape scale. *Landscape and Urban Planning*, **243**, 104973. Available from: <https://doi.org/10.1016/j.landurbplan.2023.104973>
- Atkins, J.W., Costanza, J., Dahlin, K.M., Dannenberg, M.P., Elmore, A.J., Fitzpatrick, M.C. et al. (2023) Scale dependency of lidar-derived forest structural diversity. *Methods in Ecology and Evolution*, **14**(2), 708–723. Available from: <https://doi.org/10.1111/2041-210x.14040>
- Bayle, A. (2020) A recent history of deglaciation and vegetation establishment in a contrasted geomorphological context, Glacier Blanc, French Alps. *Journal of Maps*, **16**(2), 766–775. Available from: <https://doi.org/10.1080/17445647.2020.1829115>
- Bayle, A., Carlson, B.Z., Zimmer, A., Vallée, S., Rabatel, A., Cremonese, E. et al. (2023) Local environmental context drives heterogeneity of early succession dynamics in alpine glacier forefields. *Biogeosciences*, **20**(8), 1649–1669. Available from: <https://doi.org/10.5194/bg-20-1649-2023>
- Bayle, A., Gascoin, S., Berner, L.T. & Choler, P. (2024) Landsat-based greening trends in alpine ecosystems are inflated by multidecadal increases in summer observations. *Ecography*, **2024**(12), e07394. Available from: <https://doi.org/10.21203/rs.3.rs-4153160/v2>
- Bayle, A., Roy, A., Dedieu, J.-P., Boudreau, S., Choler, P. & Lévesque, E. (2022) Two distinct waves of greening in northeastern Canada: summer warming does not tell the whole story. *Environmental Research Letters*, **17**(6), 064051. Available from: <https://doi.org/10.1088/1748-9326/ac74d6>
- Berner, L.T., Assmann, J.J., Normand, S. & Goetz, S.J. (2023) LandsatTS: an R package to facilitate retrieval, cleaning, cross-calibration, and phenological modeling of Landsat time series data. *Ecography*, **2023**(9), e06768. Available from: <https://doi.org/10.1111/ecog.06768>
- Berner, L.T. & Goetz, S.J. (2022) Satellite observations document trends consistent with a boreal forest biome shift. *Global Change Biology*, **28**(10), 3275–3292. Available from: <https://doi.org/10.1111/gcb.16121>
- Berner, L.T., Massey, R., Jantz, P., Forbes, B.C., Macias-Fauria, M., Myers-Smith, I. et al. (2020) Summer warming explains widespread but not uniform greening in the Arctic tundra biome. *Nature Communications*, **11**(1), 4621. Available from: <https://doi.org/10.1038/s41467-020-18479-5>
- Böhner, J. & Antanić, O. (2009) Chapter 8 land-surface parameters specific to topo-climatology. *Developments in Soil Science*, **33**, 195–226. Available from: [https://doi.org/10.1016/s0166-2481\(08\)00008-1](https://doi.org/10.1016/s0166-2481(08)00008-1)
- Bolton, D.K., Coops, N.C., Hermosilla, T., Wulder, M.A. & White, J.C. (2018) Evidence of vegetation greening at alpine treeline ecotones: three decades of Landsat spectral trends informed by lidar-derived vertical structure. *Environmental Research Letters*, **13**(8), 084022. Available from: <https://doi.org/10.1088/1748-9326/aad5d2>
- Bräker, O.U. (2002) Measuring and data processing in tree-ring research – a methodological introduction. *Dendrochronologia*, **20**(1–2), 203–216. Available from: <https://doi.org/10.1078/1125-7865-00017>
- Camarero, J.J., García-Ruiz, J.M., Sangüesa-Barreda, G., Galván, J.D., Alla, A.Q., Sanjuán, Y. et al. (2018) Recent and intense dynamics in a formerly static Pyrenean treeline. *Arctic, Antarctic, and Alpine Research*, **47**(4), 773–783. Available from: <https://doi.org/10.1657/aaar0015-001>
- Camarero, J.J. & Gutiérrez, E. (2004) Pace and pattern of recent Treeline dynamics: response of ecotones to climatic variability in the Spanish Pyrenees. *Climatic Change*, **63**(1/2), 181–200. Available from: <https://doi.org/10.1023/b:clim.0000018507.71343.46>
- Campion-Vincent, V. (2005) The restoration of wolves in France: story, conflicts and uses of rumor. In: Herda-Rapp, A. & Goedeke, T.L. (Eds.) *Mad about wildlife: looking at social conflict over wildlife*. Brill: Boston, MA, pp. 99–122. Available from: https://doi.org/10.1163/9789047407447_008
- Camps-Valls, G., Campos-Taberner, M., Moreno-Martinez, A., Walther, S., Duveiller, G., Cescatti, A. et al. (2021) A unified vegetation index for quantifying the terrestrial biosphere. *Science Advances*, **7**(9), eabc7447. Available from: <https://doi.org/10.1126/sciadv.abc7447>
- Cannone, N., Diolaiuti, G., Guglielmin, M. & Smiraglia, C. (2008) Accelerating climate change impacts on alpine glacier forefield ecosystems in the European Alps. *Ecological Applications*, **18**(3), 637–648. Available from: <https://doi.org/10.1890/07-1188.1>
- Cannone, N., Guglielmin, M., Casiraghi, C. & Malfasi, F. (2022) Salix shrub encroachment along a 1000 m elevation gradient triggers a major ecosystem change in the European Alps. *Ecography*, **2022**(2). Available from: <https://doi.org/10.1111/ecog.06007>
- Cannone, N., Sgorbati, S. & Guglielmin, M. (2007) Unexpected impacts of climate change on alpine vegetation. *Frontiers in Ecology and the Environment*, **5**(7), 360–364. Available from: [https://doi.org/10.1890/1540-9295\(2007\)5\[360:uiocco\]2.0.co;2](https://doi.org/10.1890/1540-9295(2007)5[360:uiocco]2.0.co;2)
- Carlson, B.Z., Corona, M.C., Dentant, C., Bonet, R., Thuiller, W. & Choler, P. (2017) Observed long-term greening of alpine vegetation—a case study in the French Alps. *Environmental Research Letters*, **12**(11), 114006. Available from: <https://doi.org/10.1088/1748-9326/aa84bd>
- Carlson, B.Z., Renaud, J., Biron, P.E. & Choler, P. (2014) Long-term modeling of the forest-grassland ecotone in the

- French Alps: implications for land management and conservation. *Ecological Applications*, **24**(5), 1213–1225. Available from: <https://doi.org/10.1890/13-0910.1>
- Chave, J. (2013) The problem of pattern and scale in ecology: what have we learned in 20 years? *Ecology Letters*, **16**(Suppl 1), 4–16. Available from: <https://doi.org/10.1111/ele.12048>
- Choler, P., Bayle, A., Carlson, B.Z., Randin, C., Filippa, G. & Cremonese, E. (2021) The tempo of greening in the European Alps: spatial variations on a common theme. *Global Change Biology*, **27**(21), 5614–5628. Available from: <https://doi.org/10.1111/gcb.15820>
- Choler, P., Bayle, A., Fort, N. & Gascoin, S. (2024) Waning snowfields have transformed into hotspots of greening within the alpine zone. *Nature Climate Change*. Available from: <https://doi.org/10.1038/s41558-024-02177-x>
- Dentant, C., Carlson, B.Z., Bartalucci, N., Bayle, A. & Lavergne, S. (2023) Anthropocene trajectories of high alpine vegetation on Mont-Blanc nunataks. *Botany Letters*, **1-15**, 65–79. Available from: <https://doi.org/10.1080/23818107.2023.2231503>
- Devi, N., Hagedorn, F., Moiseev, P., Bugmann, H., Shiyatov, S., Mazepa, V. et al. (2008) Expanding forests and changing growth forms of Siberian larch at the polar Urals treeline during the 20th century. *Global Change Biology*, **14**(7), 1581–1591. Available from: <https://doi.org/10.1111/j.1365-2486.2008.01583.x>
- Didier, L. (2001) Invasion patterns of European larch and Swiss stone pine in subalpine pastures in the French Alps. *Forest Ecology and Management*, **145**(1–2), 67–77. Available from: [https://doi.org/10.1016/S0378-1127\(00\)00575-2](https://doi.org/10.1016/S0378-1127(00)00575-2)
- Dinca, L., Nita, M., Hofgaard, A., Alados, C.L., Broll, G., Borz, S.A. et al. (2017) Forests dynamics in the montane–alpine boundary: a comparative study using satellite imagery and climate data. *Climate Research*, **73**(1–2), 97–110. Available from: <https://doi.org/10.3354/cr01452>
- Dullinger, S., Dirnböck, T. & Grabherr, G. (2003) Patterns of shrub invasion into High Mountain grasslands of the Northern Calcareous Alps, Austria. *Arctic, Antarctic, and Alpine Research*, **35**(4), 434–441. Available from: [https://doi.org/10.1657/1523-0430\(2003\)035\[0434:posiuh\]2.0.co;2](https://doi.org/10.1657/1523-0430(2003)035[0434:posiuh]2.0.co;2)
- Dullinger, S., Dirnböck, T. & Grabherr, G. (2004) Modelling climate change-driven treeline shifts: relative effects of temperature increase, dispersal and invasibility. *Journal of Ecology*, **92**(2), 241–252. Available from: <https://doi.org/10.1111/j.0022-0477.2004.00872.x>
- Eichel, J., Stoffel, M. & Wipf, S. (2023) Go or grow? Feedbacks between moving slopes and shifting plants in high mountain environments. *Progress in Physical Geography: Earth and Environment*, **47**(6), 967–985. Available from: <https://doi.org/10.1177/0309133231193844>
- Espuno, N., Lequette, B., Pouille, M.-L., Migot, P. & Lebreton, J.-D. (2004) Heterogeneous response to preventive sheep husbandry during wolf recolonization of the French Alps. *Wildlife Society Bulletin*, **32**(4), 1195–1208. Available from: [https://doi.org/10.2193/0091-7648\(2004\)032\[1195:hrtphsh\]2.0.co;2](https://doi.org/10.2193/0091-7648(2004)032[1195:hrtphsh]2.0.co;2)
- Estes, L., Elsen, P.R., Treuer, T., Ahmed, L., Caylor, K., Chang, J. et al. (2018) The spatial and temporal domains of modern ecology. *Nature Ecology & Evolution*, **2**(5), 819–826. Available from: <https://doi.org/10.1038/s41559-018-0524-4>
- Formica, A., Farrer, E.C., Ashton, I.W. & Suding, K.N. (2018) Shrub expansion over the past 62 years in Rocky Mountain Alpine Tundra: possible causes and consequences. *Arctic, Antarctic, and Alpine Research*, **46**(3), 616–631. Available from: <https://doi.org/10.1657/1938-4246-46.3.616>
- Fourchy, P. (1953) Etudes sur l'Ecologie et la Sylviculture du Mélèze.
- Francon, L., Corona, C., Till-Bottraud, I., Choler, P., Roussel, E., Carlson, B.Z. et al. (2021) Shrub growth in the Alps diverges from air temperature since the 1990s. *Environmental Research Letters*, **16**(7), 074026. Available from: <https://doi.org/10.1088/1748-9326/ac0b67>
- Francon, L., Roussel, E., Lopez-Saez, J., Saulnier, M., Stoffel, M. & Corona, C. (2023) Alpine shrubs have benefited more than trees from 20th century warming at a treeline ecotone site in the French Pyrenees. *Agricultural and Forest Meteorology*, **329**, 109284. Available from: <https://doi.org/10.1016/j.agrformet.2022.109284>
- Garbarino, M., Lingua, E., Nagel, T.A., Godone, D. & Motta, R. (2010) Patterns of larch establishment following deglaciation of Ventina glacier, central Italian Alps. *Forest Ecology and Management*, **259**(3), 583–590. Available from: <https://doi.org/10.1016/j.foreco.2009.11.016>
- Garbarino, M., Morresi, D., Anselmetto, N. & Weisberg, P.J. (2023) Treeline remote sensing: from tracking treeline shifts to multi-dimensional monitoring of ecotonal change. *Remote Sensing in Ecology and Conservation*, **9**(6), 729–742. Available from: <https://doi.org/10.1002/rse2.351>
- Gehrig-Fasel, J., Guisan, A. & Zimmermann, N.E. (2007) Tree line shifts in the Swiss Alps: climate change or land abandonment? *Journal of Vegetation Science*, **18**(4), 571–582. Available from: <https://doi.org/10.1111/j.1654-1103.2007.tb02571.x>
- Giguet-Covex, C., Pansu, J., Arnaud, F., Rey, P.J., Griggo, C., Gelly, L. et al. (2014) Long livestock farming history and human landscape shaping revealed by lake sediment DNA. *Nature Communications*, **5**, 3211. Available from: <https://doi.org/10.1038/ncomms4211>
- Gottfried, M., Pauli, H., Futschik, A., Akhalkatsi, M., Barančok, P., Benito Alonso, J.L. et al. (2012) Continent-wide response of mountain vegetation to climate change. *Nature Climate Change*, **2**(2), 111–115. Available from: <https://doi.org/10.1038/nclimate1329>
- Greenwell, B.M. (2017) pdp: an R package for constructing spatial dependence plots. *The R Journal*, **9**(1), 421–436.
- Gril, E., Laslier, M., Gallet-Moron, E., Durrieu, S., Spicher, F., Le Roux, V. et al. (2023) Using airborne LiDAR to map forest microclimate temperature buffering or amplification.

- Remote Sensing of Environment*, **298**, 113820. Available from: <https://doi.org/10.1016/j.rse.2023.113820>
- Hamid, M., Khuroo, A.A., Malik, A.H., Ahmad, R., Singh, C.P., Dolezal, J. et al. (2020) Early evidence of shifts in Alpine summit vegetation: a case study from Kashmir Himalaya. *Frontiers in Plant Science*, **11**, 421. Available from: <https://doi.org/10.3389/fpls.2020.00421>
- Harsch, M.A., Hulme, P.E., McGlone, M.S. & Duncan, R.P. (2009) Are treelines advancing? A global meta-analysis of treeline response to climate warming. *Ecology Letters*, **12**(10), 1040–1049. Available from: <https://doi.org/10.1111/j.1461-0248.2009.01355.x>
- Ives, A.R., Zhu, L., Wang, F., Zhu, J., Morrow, C.J. & Radeloff, V.C. (2021) Statistical inference for trends in spatiotemporal data. *Remote Sensing of Environment*, **266**, 112678. Available from: <https://doi.org/10.1016/j.rse.2021.112678>
- Kucsicsa, G. & Bălteanu, D. (2020) The influence of man-induced land-use change on the upper forest limit in the Romanian Carpathians. *European Journal of Forest Research*, **139**(6), 893–914. Available from: <https://doi.org/10.1007/s10342-020-01293-5>
- Kuhn, M., Wing, J., Weston, S., Williams, A., Keefer, C., Engelhardt, A. et al. (2023) R Package ‘Caret’: Classification and Regression Training.
- Lamprecht, A., Semenchuk, P.R., Steinbauer, K., Winkler, M. & Pauli, H. (2018) Climate change leads to accelerated transformation of high-elevation vegetation in the central Alps. *The New Phytologist*, **220**(2), 447–459. Available from: <https://doi.org/10.1111/nph.15290>
- Larsson, L. (2013) Coorecorder and Cdendro Programs of the Coorecorder/Cdendropackage. <http://www.cybis.se/forfun/dendro>
- Liang, E., Wang, Y., Eckstein, D. & Luo, T. (2011) Little change in the fir tree-line position on the southeastern Tibetan Plateau after 200 years of warming. *The New Phytologist*, **190**(3), 760–769. Available from: <https://doi.org/10.1111/j.1469-8137.2010.03623.x>
- Liaw, A. & Wiener, M. (2002) Classification and regression by randomForest. *R News*, **2**(3), 18–22.
- Malfasi, F. & Cannone, N. (2020) Climate warming persistence triggered tree ingressation after shrub encroachment in a high alpine tundra. *Ecosystems*, **23**(8), 1657–1675. Available from: <https://doi.org/10.1007/s10021-020-00495-7>
- Mather, A.S., Fairbairn, J. & Needle, C.L. (1999) The course and drivers of the forest transition: the case of France. *Journal of Rural Studies*, **15**(1), 65–90. Available from: [https://doi.org/10.1016/s0743-0167\(98\)00023-0](https://doi.org/10.1016/s0743-0167(98)00023-0)
- Meyfroidt, P. & Lambin, E.F. (2011) Global Forest transition: prospects for an end to deforestation. *Annual Review of Environment and Resources*, **36**(1), 343–371. Available from: <https://doi.org/10.1146/annurev-environ-090710-143732>
- Meyfroidt, P., Rudel, T.K. & Lambin, E.F. (2010) Forest transitions, trade, and the global displacement of land use. *Proceedings of the National Academy of Sciences of the United States of America*, **107**(49), 20917–20922. Available from: <https://doi.org/10.1073/pnas.1014773107>
- Morton, D.C., Nagol, J., Carabajal, C.C., Rosette, J., Palace, M., Cook, B.D. et al. (2014) Amazon forests maintain consistent canopy structure and greenness during the dry season. *Nature*, **506**(7487), 221–224. Available from: <https://doi.org/10.1038/nature13006>
- Myers-Smith, I.H., Forbes, B.C., Wilmking, M., Hallinger, M., Lantz, T., Blok, D. et al. (2011) Shrub expansion in tundra ecosystems: dynamics, impacts and research priorities. *Environmental Research Letters*, **6**(4), 045509. Available from: <https://doi.org/10.1088/1748-9326/6/4/045509>
- Myers-Smith, I.H., Kerby, J.T., Phoenix, G.K., Bjerke, J.W., Epstein, H.E., Assmann, J. et al. (2020) Complexity revealed in the greening of the Arctic. *Nature Climate Change*, **10**(2), 106–117. Available from: <https://doi.org/10.1038/s41558-019-0688-1>
- Nagol, J.R., Sexton, J.O., Kim, D.-H., Anand, A., Morton, D., Vermote, E. et al. (2015) Bidirectional effects in Landsat reflectance estimates: is there a problem to solve? *ISPRS Journal of Photogrammetry and Remote Sensing*, **103**, 129–135. Available from: <https://doi.org/10.1016/j.isprsjprs.2014.09.006>
- Oliver, C.D. & Larson, B.C. (1996) Forest stand dynamics.
- Pauli, H., Gottfried, M., Dullinger, S., Abdaladze, O., Akhalkatsi, M., Benito Alonso, J.L. et al. (2012) Recent plant diversity changes on Europe’s mountain summits. *Science*, **336**(6079), 353–355. Available from: <https://doi.org/10.1126/science.1219033>
- Pepin, N.C., Arnone, E., Gobiet, A., Haslinger, K., Kotlarski, S., Notarnicola, C. et al. (2022) Climate changes and their Elevational patterns in the mountains of the world. *Reviews of Geophysics*, **60**(1), e2020RG000730. Available from: <https://doi.org/10.1029/2020rg000730>
- Pepin, N.C., Bradley, R.S., Diaz, H.F., Baraer, M., Caceres, E.B., Forsythe, N. et al. (2015) Elevation-dependent warming in mountain regions of the world. *Nature Climate Change*, **5**(5), 424–430. Available from: <https://doi.org/10.1038/nclimate2563>
- Pettorelli, N., Laurance, W.F., O’Brien, T.G., Wegmann, M., Nagendra, H., Turner, W. et al. (2014) Satellite remote sensing for applied ecologists: opportunities and challenges. *Journal of Applied Ecology*, **51**(4), 839–848. Available from: <https://doi.org/10.1111/1365-2664.12261>
- Pini, R., Ravazzi, C., Raiteri, L., Guerreschi, A., Castellano, L., Comolli, R. et al. (2017) From pristine forests to high-altitude pastures: an ecological approach to prehistoric human impact on vegetation and landscapes in the western Italian Alps. *Journal of Ecology*, **105**(6), 1580–1597. Available from: <https://doi.org/10.1111/1365-2745.12767>
- Rogora, M., Frate, L., Carranza, M.L., Freppaz, M., Stanisci, A., Bertani, I. et al. (2018) Assessment of climate change effects on mountain ecosystems through a cross-site analysis

- in the Alps and Apennines. *Science of the Total Environment*, **624**, 1429–1442. Available from: <https://doi.org/10.1016/j.scitotenv.2017.12.155>
- Roussel, J.-R., Auty, D., Coops, N.C., Tompalski, P., Goodbody, T.R.H., Meador, A.S. et al. (2020) lidR: an R package for analysis of airborne laser scanning (ALS) data. *Remote Sensing of Environment*, **251**, 112061. Available from: <https://doi.org/10.1016/j.rse.2020.112061>
- Roy, D.P., Zhang, H.K., Ju, J., Gomez-Dans, J.L., Lewis, P.E., Schaaf, C.B. et al. (2016) A general method to normalize Landsat reflectance data to nadir BRDF adjusted reflectance. *Remote Sensing of Environment*, **176**, 255–271. Available from: <https://doi.org/10.1016/j.rse.2016.01.023>
- Rumpf, S.B., Gravey, M., Bronnimann, O., Luoto, M., Cianfrani, C., Mariethoz, G. et al. (2022) From white to green: snow cover loss and increased vegetation productivity in the European Alps. *Science*, **376**(6597), 1119–1122. Available from: <https://doi.org/10.1126/science.abn6697>
- Schaaf, C.B., Gao, F., Strahler, A.H., Lucht, W., Li, X., Tsang, T. et al. (2002) First operational BRDF, albedo nadir reflectance products from MODIS. *Remote Sensing of Environment*, **83**(1–2), 135–148. Available from: [https://doi.org/10.1016/S0034-4257\(02\)00091-3](https://doi.org/10.1016/S0034-4257(02)00091-3)
- Schumann, K., Gewolf, S. & Tackenberg, O. (2016) Factors affecting primary succession of glacier foreland vegetation in the European Alps. *Alpine Botany*, **126**(2), 105–117. Available from: <https://doi.org/10.1007/s00035-016-0166-6>
- Tasser, E., Walde, J., Tappeiner, U., Teutsch, A. & Nogler, W. (2007) Land-use changes and natural reforestation in the Eastern Central Alps. *Agriculture, Ecosystems & Environment*, **118**(1–4), 115–129. Available from: <https://doi.org/10.1016/j.agee.2006.05.004>
- Timoney, K. (2022) Letter to the editor on “Satellite observations document trends consistent with a boreal biome shift”. *Global Change Biology*, **28**(10), 3275–3292. Available from: <https://doi.org/10.1111/gcb.16121>
- Treml, V., Šenfeldr, M., Chuman, T., Ponocná, T., Demková, K. & Collins, B. (2016) Twentieth century treeline ecotone advance in the Sudetes Mountains (Central Europe) was induced by agricultural land abandonment rather than climate change. *Journal of Vegetation Science*, **27**(6), 1209–1221. Available from: <https://doi.org/10.1111/jvs.12448>
- van Ewijk, K.Y., Treitz, P.M. & Scott, N.A. (2011) Characterizing Forest succession in Central Ontario using Lidar-derived indices. *Photogrammetric Engineering & Remote Sensing*, **77**(3), 261–269. Available from: <https://doi.org/10.14358/pers.77.3.261>
- Vitali, A., Urbinati, C., Weisberg, P.J., Urza, A.K., Garbarino, M. & Kikvidze, Z. (2018) Effects of natural and anthropogenic drivers on land-cover change and treeline dynamics in the Apennines (Italy). *Journal of Vegetation Science*, **29**(2), 189–199. Available from: <https://doi.org/10.1111/jvs.12598>
- Vitasse, Y., Ursenbacher, S., Klein, G., Bohnenstengel, T., Chittaro, Y., Delestrade, A. et al. (2021) Phenological and elevational shifts of plants, animals and fungi under climate change in the European Alps. *Biological Reviews of the Cambridge Philosophical Society*, **96**(5), 1816–1835. Available from: <https://doi.org/10.1111/brv.12727>
- Vittoz, P., Bodin, J., Ungricht, S., Burga, C.A. & Walther, G.R. (2008) One century of vegetation change on Isla Persa, a nunatak in the Bernina massif in the Swiss Alps. *Journal of Vegetation Science*, **19**(5), 671–680. Available from: <https://doi.org/10.3170/2008-8-18434>
- Vittoz, P., Rulence, B., Largey, T. & Freléchoux, F. (2008) Effects of climate and land-use change on the establishment and growth of Cembran pine (*Pinus cembra* L.) over the altitudinal Treeline ecotone in the central Swiss Alps. *Arctic, Antarctic, and Alpine Research*, **40**(1), 225–232. Available from: [https://doi.org/10.1657/1523-0430\(06-010\)\[vittoz\]2.0.co;2](https://doi.org/10.1657/1523-0430(06-010)[vittoz]2.0.co;2)
- Walsh, K. (2015) Risk and marginality at high altitudes: new interpretations from fieldwork on the Faravel Plateau, Hautes-Alpes. *Antiquity*, **79**(304), 289–305. Available from: <https://doi.org/10.1017/S0003598X00114097>
- Wei, C., Karger, D.N. & Wilson, A.M. (2020) Spatial detection of alpine treeline ecotones in the Western United States. *Remote Sensing of Environment*, **240**, 111672. Available from: <https://doi.org/10.1016/j.rse.2020.111672>
- Wong, C.M. & Lertzman, K.P. (2001) Errors in estimating tree age: implications for studies of stand dynamics. *Canadian Journal of Forest Research*, **31**(7), 1262–1271. Available from: <https://doi.org/10.1139/cjfr-31-7-1262>
- Yin, G., Xie, J., Ma, D., Xie, Q., Verger, A., Descals, A. et al. (2023) Aspect matters: unraveling microclimate impacts on mountain greenness and greening. *Geophysical Research Letters*, **50**(24), e2023GL105879. Available from: <https://doi.org/10.1029/2023gl105879>
- Zhang, H.K., Roy, D.P. & Kovalskyy, V. (2016) Optimal solar geometry definition for global long-term Landsat time-series bidirectional reflectance normalization. *IEEE Transactions on Geoscience and Remote Sensing*, **54**(3), 1410–1418. Available from: <https://doi.org/10.1109/tgrs.2015.2480684>
- Zhu, Z., Wang, S. & Woodcock, C.E. (2015) Improvement and expansion of the Fmask algorithm: cloud, cloud shadow, and snow detection for Landsats 4–7, 8, and sentinel 2 images. *Remote Sensing of Environment*, **159**, 269–277. Available from: <https://doi.org/10.1016/j.rse.2014.12.014>
- Zhu, Z. & Woodcock, C.E. (2012) Object-based cloud and cloud shadow detection in Landsat imagery. *Remote Sensing of Environment*, **118**, 83–94. Available from: <https://doi.org/10.1016/j.rse.2011.10.028>
- Zimmer, A., Meneses, R.I., Rabatel, A., Soruco, A., Dangles, O. & Anthelme, F. (2018) Time lag between glacial retreat and upward migration alters tropical alpine communities. *Perspectives in Plant Ecology, Evolution and Systematics*, **30**, 89–102. Available from: <https://doi.org/10.1016/j.ppees.2017.05.003>